Simulation Topology, Important Parameters, and TM-DIO Detailed Process

This document provides the topology diagram of the modified IEEE 10-machine 39-bus system, the detailed process of the TM-DIO method, as well as important parameters for the physical system, control, the KA&EL-EA algorithm, data-driven training, and both high and low wind speed scenarios.

The topology diagram of the modified IEEE 10-machine 39-bus system is shown in Fig. 1:

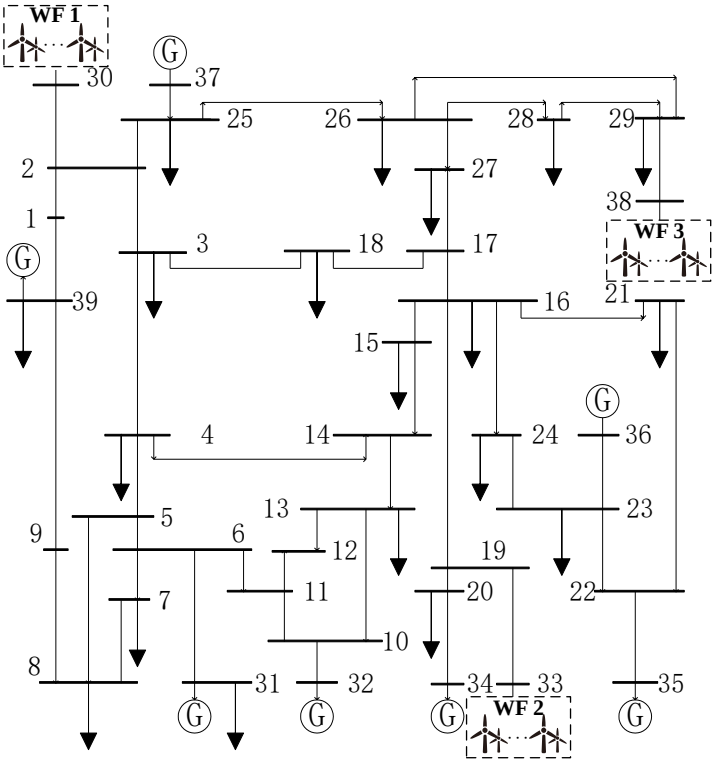

Fig. 1 IEEE 39-bus test system with three wind farms.

The system and control parameters are shown in Table I:

TABLE I

SYSTEM AND CONTROL PARAMETERS

Parameter Name	Value
PFR Optimization period	20 s
Sampling period	0.01 s
System nominal frequency	50 Hz
the maximum frequency deviation limit	0.5 Hz
the maximum RoCoF limit	0.6 Hz/s
the maximum QSSFD limit	0.25 Hz
The security range of node voltage	[0.92, 1.08] p.u.
the upper limit of branch power	0.133 p.u.

the PFR energy compensation price of WF1	\$50/MWh
the PFR energy compensation price of WF2	\$100/MWh
the PFR energy compensation price of WF3	\$150/MWh
the inertia coefficient compensation price of WF1	\$0.04/(MW·s/Hz)
the inertia coefficient compensation price of WF2	\$0.1/(MW·s/Hz)
the inertia coefficient compensation price of WF3	\$0.15/(MW·s/Hz)

The parameters of the conventional thermal generators are shown in Table II:

TABLE II

PARAMETERS OF THE CONVENTIONAL THERMAL GENERATORS

Generator Node Location	Output Power	H_g	R_g	T_g(s)	F_g	K_g	D
31	92 MW	4.4	0.0891	4.0719	0.2185	1	2.8508
32	93.6 MW	4.4	0.0658	5.0300	0.2070	1	2.8508
34	94.4 MW	4.4	0.0891	4.3115	0.2875	1	2.8508
35	88 MW	4.4	0.0891	2.8743	0.3450	1	2.8508
36	84 MW	4.4	0.0802	6.7067	0.3565	1	2.8508
37	89.6 MW	4.4	0.0668	5.7486	0.3680	1	2.8508
39	99.726 MW	4.4	0.0608	5.7486	0.3680	1	2.8508

The parameters of WT are shown in Table III:

TABLE III

PARAMETERS OF WT

Parameter Name	Value
Rated power	6 MW
Maximum limit speed	1.3 p.u.
Minimum limit speed	0.7 p.u.
Maximum power output	6.3 MW
Rotational inertia	192000000 kg·m^2
Blade pitch angle	0°
Swept area of WT blades	12076 m^2
Converter response time	1.2 s

The parameters of the KA&EL-EA algorithm are shown in Table IV:

TABLE IV

PARAMETERS OF KA&EL-EA ALGORITHM

Parameter	Value
n_p	50
MaxIt	100
w_{max}	0.9
w_{min}	0.2
δ'	0.1
$\bar{\boldsymbol{u}}$	[50,50,50,30,30,30]

$\underline{\boldsymbol{u}}$	[0,0,0,0,0,0]
n_{mut}	50
σ'	1e-5

The wind speeds of three WFs under low wind speed and high wind speed test scenarios are shown in Table V to Table. VII:

TABLE V

WIND SPEED DATA OF WIND FARM 1

Scenarios	Anemometer tower 1	Anemometer tower 2	Anemometer tower 3
Low wind speed	8.8712	8.9152	8.8421
High wind speed	10.0033	10.0411	10.0358

TABLE VI

WIND SPEED DATA OF WIND FARM 2

Scenarios	Anemometer tower 1	Anemometer tower 2	Anemometer tower 3	Anemometer tower 4
Low wind speed	8.7211	8.5947	8.3774	8.2400
High wind speed	10.002	10.0883	10.0032	10.0542

TABLE VII

WIND SPEED DATA OF WIND FARM 3

Scenarios	Anemometer tower 1	Anemometer tower 2	Anemometer tower 3	Anemometer tower 4	Anemometer tower 5
Low wind speed	8.4145	8.3891	8.4523	8.1056	8.2357
High wind speed	10.60211	10.6964	10.4502	10.3812	10.5229

The requirements of data-driven training are shown in Table VIII:

TABLE VIII

REQUIREMENTS OF DATA QUALITY

Number of historical samples	1599
Number of augmented dimensions	100
The sampling time interval of training sample for WT output power	0.1 s

The 12 data-driven performance test scenarios with different wind speeds and PFR characteristics of WFs are shown in Fig. 2 to Fig. 3:

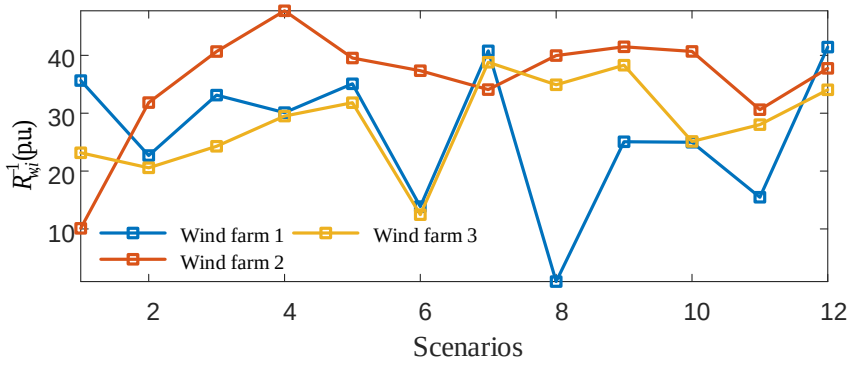

(a)

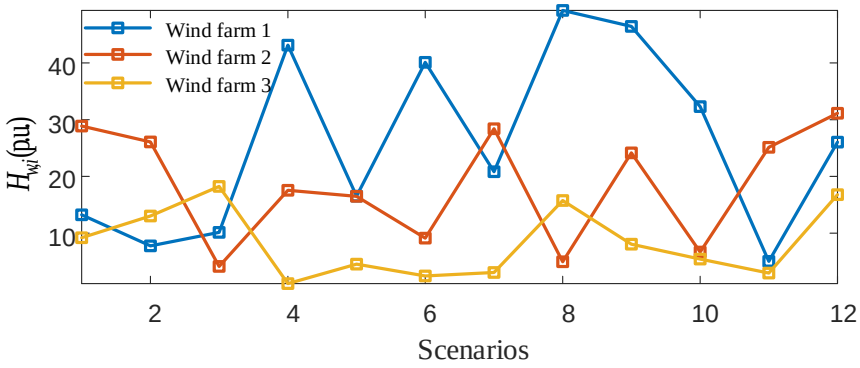

(b)

Fig. 2. The PFR characteristics of three WFs in 12 test scenarios

(a) Droop coefficient (b) Inertia coefficient

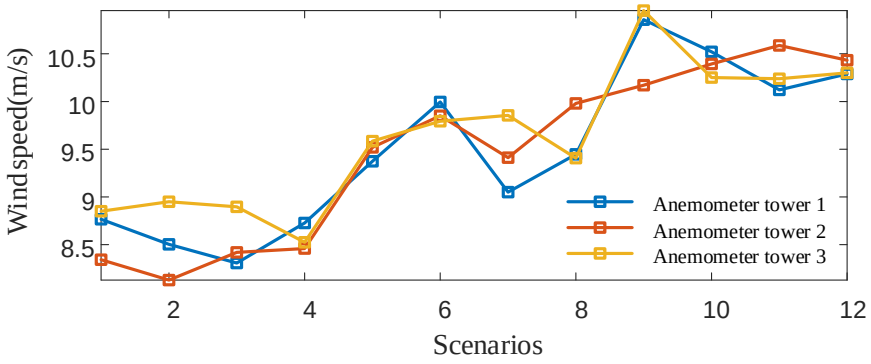

(a)

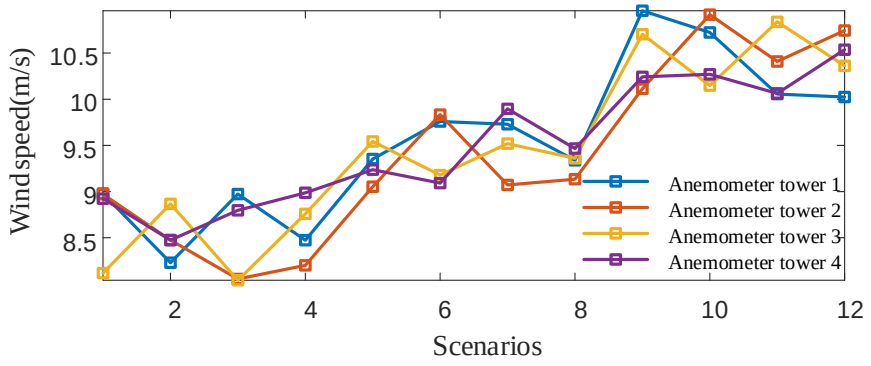

(b)

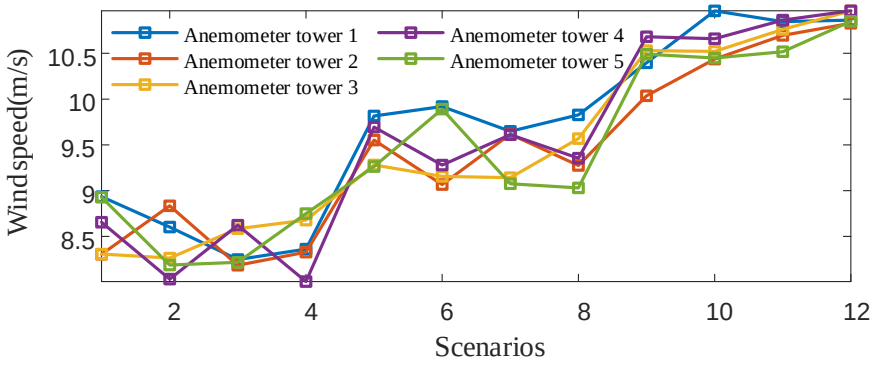

(c)

Fig. 3. The wind speeds of three WFs in 12 test scenarios

(a) Wind farm 1 (b) Wind farm 2 (c) Wind farm 3

The specific process of the TM-DIO method can be summarized as follows:

1) Each wind farm calculates its feasible domain for inertia/droop coefficient based on real-time operational data, utilizing a dual-loop traversal method within the FSC time-series physical coupling model (21), and reports the results to the bulk grid. 2) Upon receiving the feasible domains for inertia/droop coefficients from all wind farms, the KA&EL-EA method is employed for optimizing the scheduling of multi-wind farm frequency regulation characteristics, with the allocation results for inertia/droop coefficients redistributed to each wind farm. 3) Repeat the process until convergence criterion is satisfied:

$$\begin{cases} \left|R_w(t+1)-R_w(t)\right| \le \rho_1 \\ \left|H_w(t+1)-H_w(t)\right| \le \rho_2 \\ \left|R_{w,i}(t+1)-R_{w,i}(t)\right| \le \rho_3, \text{for all } i \in \{1,2,\cdots,n\} \\ \left|H_{w,i}(t+1)-H_{w,i}(t)\right| \le \rho_4, \text{for all } i \in \{1,2,\cdots,n\} \end{cases}$$

where ρ_1, ρ_2, ρ_3 and ρ_4 denote the tolerance.

The detailed process of utilizing a dual-loop traversal method within the FSC time-series physical coupling model (21) to determine the feasible domain for the frequency regulation capability of wind farms is illustrated in Fig. 4, using the *i*-th wind farm as an example:

1) Receive the inertia coefficients and droop coefficients of all wind farms excluding *i*-th wind farm.

2) Define all possible values for $H_{w,i}$ as $H_{w,i}^*(1)$ to $H_{w,i}^*(m')$, and for $R_{w,i}$ as $R_{w,i}^*(1)$ to $R_{w,i}^*(n')$. Set the counting variables i' and j', initializing $i'=1$.

3) Check if i' is less than or equal to m'. If true, set $j'=1$ and proceed to step (4); if false, the algorithm concludes.

4) Check if j' is less than or equal to n'. If true, proceed to step (5); if false, increment i' by 1 and return to step (2).

5) Substitute $H_{w,i}^*(i')$ and $R_{w,i}^*(j')$ into equation (21) in the original paper for calculation. If the condition is satisfied, proceed to step (6); if not, increment j' by 1 and return to step (4).

6) Record the coordinates ($H_{w,i}^{*}(i')$, $R_{w,i}^{*}(j')$) with $H_{w,i}$ on the x-axis and $R_{w,i}$ on the y-axis, then increment j' by 1 and return to step (3).

By following the aforementioned algorithmic steps, all feasible solutions for the virtual inertia $H_{w,i}$ and droop coefficient $R_{w,i}$ can be recorded on a two-dimensional plane, forming the feasible domain for the virtual inertia $H_{w,i}$ and droop coefficient $R_{w,i}$ of the *i*-th wind farm. This feasible domain will be reported to the bulk grid dispatch as the safety boundary for the frequency regulation capability of the *i*-th wind farm.

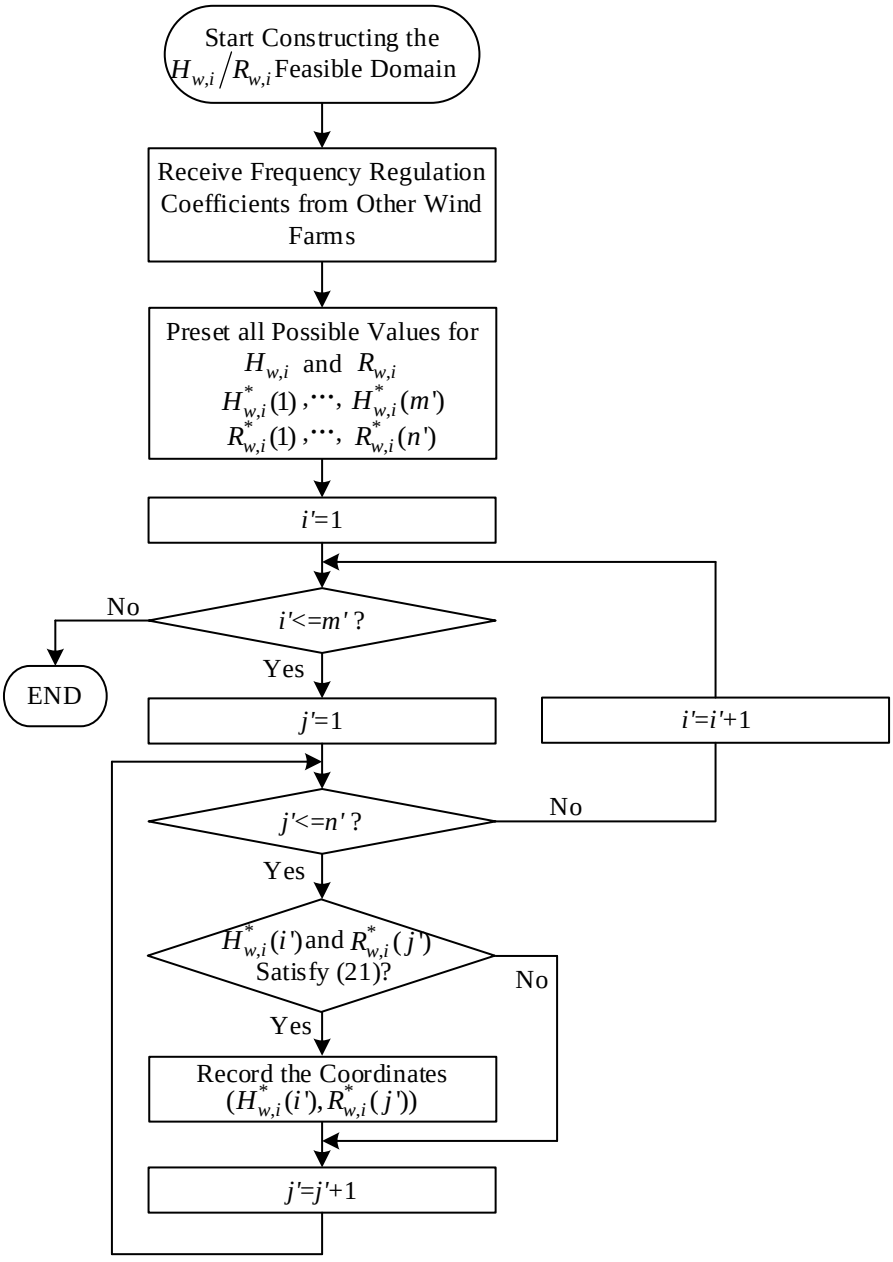

Fig. 4. FSC feasible region evaluation of wind farms based on dual-loop traversal